Carbon Vol. 17, pp. 209–222

0008–6223/79/0601–0209/$02.00/0

GALVANOMAGNETIC EFFECTS IN GRAPHITE

IAN L. SPAIN†
Engineering Materials Program, Department of Chemical Engineering and Institute for Physical Science and Technology, University of Maryland, College Park, MD 20742, U.S.A.

(*Received* 25 *August* 1978)

Abstract—A summary is given of recent work on galvanomagnetic effects in highly oriented pyrolytic graphite with current flow in the basal planes and magnetic field parallel to the *c*-axis. Experimental studies over a wide range of field are considered (0.001–23*T*) including the effect of fast neutron irradiation (0–2.9×10^{17} nvt ($E > 1$ MeV)). Theoretically, the effects of the variation of carrier properties along the zone edge, and trigonal warping of the constant energy surfaces are considered, and comparison made with predictions of the simple two band model usually used to describe galvanomagnetic properties.

1. INTRODUCTION

The purpose of this paper is to describe briefly recent advances made in our understanding and application of galvanomagnetic properties of graphite. Some of this work has appeared in greater detail in other publications [1–6]. In this paper, an overview of our studies will be given, with attention drawn to the main principles and results.

The study has included detailed measurements of the galvanomagnetic coefficients of highly oriented pyrolytic graphite (HOPG) with electronic properties similar in many respects to purified natural single crystals (SCG) or Kish graphite (KG). Defects have been introduced by fast-neutron irradiation, and galvanomagnetic effects have been used to study the resulting changes in electronic properties. Measurements have been made to very high magnetic fields (23*T* = 230 kg), into a region known as the extreme quantum limit, where new, weak, oscillations have been found.

The electronic energy states of graphite have been studied extensively by many workers. A detailed dispersion relationship for the free carriers is available [7] together with a model for the energy states in a magnetic field [8, 9]. The detailed model will be referred to as SWMcC (Slonczewski–Weiss–McClure). Most recent estimates of the band parameters can be found in Ref. [10].

The complete description of the free carriers is complicated. Electron and hole states lie along the edge of the Brillouin zone resembling highly elongated cigars. However, the surfaces are trigonally warped and the dynamic properties of the carriers (e.g. effective masses) vary strongly along the zone edge. A brief description of work to examine the effects of these complications on the galvanomagnetic coefficients will be given.

This paper will only consider effects with the current flowing perpendicular to the *c*-axis, along the layer planes. The subject of *c*-axis properties is highly contentious, because measured properties depend strongly on sample material [11]. For the work described in this paper, properties obtained on different materials such as SCG [12], KG [13] or HOPG [14] are very similar, and differences can be related to different types of scattering, resulting from different types of predominant defect.

2. PHENOMENOLOGY OF GALVANOMAGNETIC EFFECTS [15]

Since graphite has a six-fold symmetry axis the magnetoresistance and Hall effect do not depend on the direction of current within the planes. However, the magnetoresistance is strongly dependent on the direction of the applied magnetic field. In this paper, only effects with field parallel to the *c*-axis will be considered ($B \equiv B_z$).

With current flow along the *x*-direction, the measured resistivity will be denoted ρ_{xx} and the magnetoresistance $\Delta\rho/\rho_0 \equiv (\rho_{xx}(B) - \rho_{xx}(0))/\rho_{xx}(0)$. The Hall resistivity, ρ_{yx}, is:

$$\rho_{yx} = E_y/j_x \tag{1}$$

where E_y is the field developed across the sample and j_x is the current density, The Hall coefficient, R_H, is

$$R_H = \rho_{yx}/B_z. \tag{2}$$

Theoretical models give results in terms of conductivities, σ_{xx} and σ_{xy}. Experimental data on resistivities may be inverted to give conductivities using

$$\sigma_{xx} = \frac{\rho_{xx}}{\rho_{xx}^2 + \rho_{yx}^2} \tag{3a}$$

$$\sigma_{xy} = \frac{\rho_{yx}}{\rho_{xx}^2 + \rho_{yx}^2}. \tag{3b}$$

In zero field, $\rho_{yx} \to 0$, since R_H is constant in very low field (see eqn 2). Thus, from (3), $\rho_{xx}(0) = \sigma_{xx}^{-1}(0)$, and $\sigma_{xy}(0) = 0$. The resistivities can be obtained from conductivities using

$$\rho_{xx} = \frac{\sigma_{xx}}{\sigma_{xx}^2 + \sigma_{xy}^2} \tag{4a}$$

$$\rho_{yx} = \frac{\sigma_{xy}}{\sigma_{xx}^2 + \sigma_{xy}^2}. \tag{4b}$$

†Present address: Department of Physics, Colorado State University, Fort Collins, CO 80523, U.S.A.

Galvanomagnetic effects are used to estimate the densities and mobilities of carriers in the conductor. In order to understand this, a simple model of galvanomagnetic effects will be discussed.

3. SIMPLE THEORY FOR GALVANOMAGNETIC EFFECTS [15]

In the absence of a magnetic field, an applied electric field accelerates the charge carriers parallel to $\vec{E}$. Collisions of the charge carriers with lattice imperfections such as (thermal) atomic vibrations, dislocations, vacancies, impurities, produce a steady-flow current in which the charge carriers have a net average speed $\langle v \rangle$ parallel to the field. The mobility (μ) is the ratio of this average speed to the field.

$$\mu = \langle v \rangle / E \tag{5}$$

The mobility is related to the effective mass of the charge carrier m^*, and the average time between collisions τ, called the relaxation time:

$$\mu = \frac{e\tau}{m^*} = \frac{e\lambda}{m^*\langle \bar{v} \rangle} \tag{6}$$

where λ is the mean distance travelled between collisions (mean free path), and $\bar{v}$ is the average speed of the carriers, which is much greater than the drift velocity.

If the density of charge carriers is n, then the conductivity, σ, is

$$\sigma = ne\mu = \frac{ne^2\tau}{m^*} = \frac{ne^2\lambda}{m^*\langle \bar{v} \rangle}. \tag{7}$$

Many of the galvanomagnetic properties of graphite can be understood qualitatively in terms of a simple two-band model (STB), comprising a band of electrons and one of holes. The conductivities are additive. For instance

$$\sigma_{xx}(0) = n_1 e\mu_1 \text{ (electrons)} + n_2 e\mu_2 \text{ (holes)}. \tag{8}$$

When a magnetic field is applied, the combined force on a carrier due to crossed electric ($\vec{E}$) and magnetic ($\vec{B}$) fields is:

$$F = -e[\vec{E} + \vec{v} \wedge \vec{B}]. \tag{9}$$

where $\vec{v}$ is the instantaneous velocity. The action of the magnetic field is therefore to apply a force tangential to $\vec{v}$, thus producing a helicoidal motion of the carrier. It is this force which gives rise to the Hall potential and the magnetoresistance.

Simple theory gives the following forms for σ_{xx} and σ_{xy} in the semi-classical limit:

$$\sigma_{xx} = \frac{n_1 e\mu_1}{1+(\mu_1 B)^2} + \frac{n_2 e\mu_2}{1+(\mu_2 B)^2} \tag{10a}$$

$$\sigma_{xy} = \frac{-n_1 e\mu_1^2 B}{1+(\mu_1 B)^2} + \frac{n_2 e\mu_2^2 B}{1+(\mu_2 B)^2}. \tag{10b}$$

Using these formulae with the transformations (4a) and (4b) the formula for the magnetoresistance factorises exactly to give:

$$\frac{\Delta\rho}{\rho_0} = \frac{\dfrac{(1+b)^2 n_1 n_2 b}{(n_1+n_2 b)^2}\mu^2 B^2}{\left[\left(\dfrac{n_1-n_2}{n_1+bn_2}\right)^2 b^2\mu_1^2 B^2 + 1\right]} \tag{11}$$

where b is the ratio of hole to electron mobility ($b = \mu_2/\mu_1$). The expression for the Hall coefficient does not factorise readily and is too lengthy to reproduce here. In zero field

$$R_H = \frac{-1}{n_1 e}\frac{(a-b^2)}{(a+b)^2} \tag{12}$$

where $a = n_1/n_2$.

The behavior in high magnetic fields is also of interest. For the conductivities, high fields are implied when $\mu_1 B$ and $\mu_2 B$ are very much greater than unity. In this case (eqns 10a and 10b),

$$\sigma_{xx} \to e\left(\frac{n_1}{\mu_1} + \frac{n_2}{\mu_2}\right)/B^2 \tag{13}$$

$$\sigma_{xy} \to \frac{e}{B}(n_2 - n_1). \tag{14}$$

The field dependences of σ_{xx}, σ_{xy}, ρ_{xx}, ρ_{yx} are plotted in Fig. 1 for a two band model. Detailed analysis of galvanomagnetic data [12, 14, 16] suggests that $n_1 \sim n_2$, $\mu_1 \sim \mu_2$. Accordingly, the values $n_1 = 1.02n_2$, $\mu_2 = 1.1\mu_1$ are assumed in these figures. At low field σ_{xy} and ρ_{yx} are positive, becoming negative at high field, since $n_1 > n_2$.

It is interesting to compare the reduced field values at which these quantities change from behavior characteristic of low field ($\bar{\mu}B < 1$) to that of asymptotic high field behavior. σ_{xx} assumes a B^{-2} dependence for $\bar{\mu}B \geqslant 3$, while σ_{xy} reaches its limiting behavior, αB^{-1}, for somewhat higher fields. It is interesting to note that field dependences predicted for σ_{xx} and σ_{xy} in this high field limit are also predicted for less restrictive models in the semi-classical limit. Also, (14) may be used to determine the difference in densities of carriers of opposite sign for cases where there are multiple groups of carriers, warped energy surfaces, etc. In this case $(n_2 - n_1)$ is replaced by $(N - P)$ where N is the total electron density and P the total hole density.

The high field conditions are much more restrictive for resistivities than conductivities as can be seen from Fig. 1. According to (11), if the denominator becomes much greater than unity, then the magnetoresistance tends to a constant value. Also, at sufficiently high field (Fig. 1), ρ_{yx} should become linear in field and

$$|\rho_{yx}| \gg \rho_{xx}. \tag{15}$$

In this case, from (3), (4), (10a), (10b),

$$R_H \to \frac{1}{e(n_2 - n_1)}. \tag{16}$$

As will be discussed in the following, (15) is never obeyed in graphite, so that σ_{xy} data must be used to evaluate differences in carrier densities, rather than (16).

In summary, the two band model affords a useful basis against which to compare experimental data. However, it will be shown that the model is inadequate in several ways. When comparing experimental results with models, it is preferable to compare conductivities rather than resistivities, not only because the formulae are simpler, but also because "high field conditions" are reached more easily.

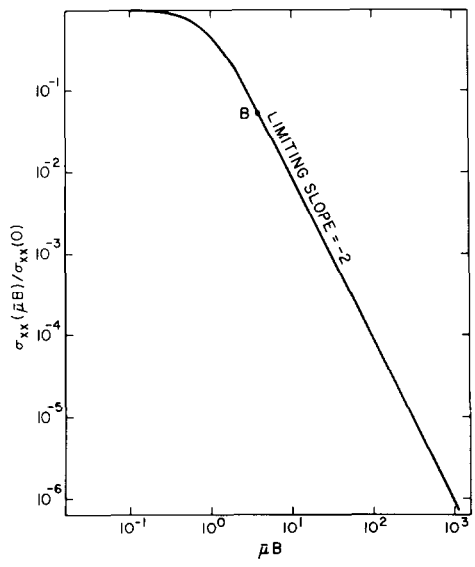

1(a)

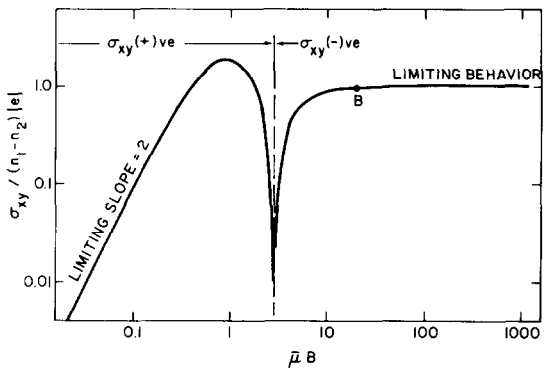

1(b)

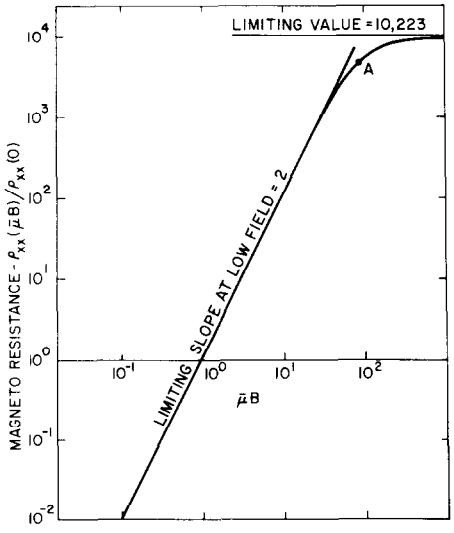

1(c)

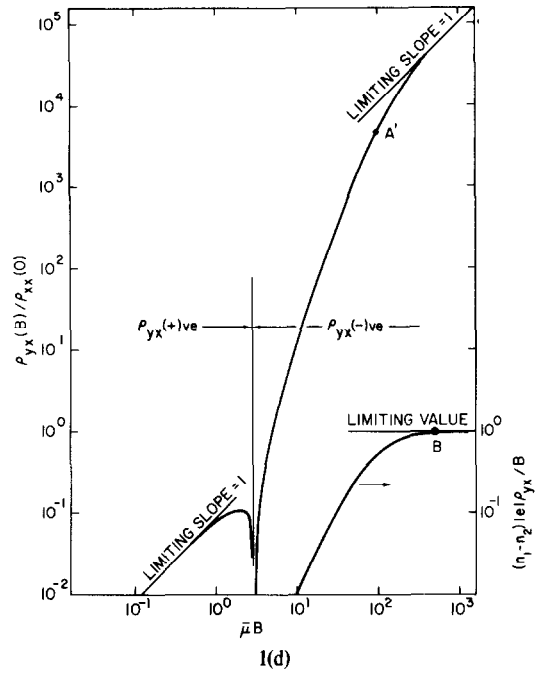

1(d)

Fig. 1. Calculated variation of galvanomagnetic quantities with magnetic field for the simple two band model (STBM) with $n_1 = 1.02\mu_2$, $\mu_2 = 1.1\mu_1$. (a), Reduced logarithmic plot for $\sigma_{xx}(B)$. Point B is approximately where the slope reaches its limiting value of -2. (b), Reduced logarithmic plot of $\sigma_{xy}(B)$. At point B σ_{xy} reaches 99% of its limiting behavior. (c), Logarithmic plot of the magnetoresistance. At point A, $|\rho_{yx}| = \rho_{xx}$. ρ_{xx} does not reach 99% of its saturation value until $\bar{\mu}B \sim 10^4$. (d), Reduced plot of ρ_{yx}. At $A'|\rho_{yx}| = \rho_{xx}$. At point B on the reduced Hall coefficient curve, this parameter has reached 99% of its saturation value. $\bar{\mu}$ is defined in eqn (22).

The reduced fields, $\bar{\mu}B$, on $\bar{\mu}B$ defined in Table 1 are useful quantities for plotting galvanomagnetic data. They are dimensionless when SI units are used (μ – $m^2\,volt^{-1}\,sec^{-1}$; B-Tesla ($IT \equiv 10\,kG$)). When $\bar{\mu}B = 1$, then, on an average, carriers complete a cyclotron orbit before being scattered. Since $\bar{\mu}$ varies strongly with temperature, the field, $B^* = 1/\bar{\mu}$, also varies, as sketched in Fig. 2, for a high quality sample of HOPG.

There are other fields which are important for the description of galvanomagnetic properties. When a field is applied, the energy levels become quantized, with a separation of $\hbar eB/m^*$. This quantisation into magnetic energy levels, called Landau levels, gives rise to ocillations in the galvanomagnetic properties at low temperature, called the Shubnikov–de Haas ocillations. When the separation between the Landau levels is greater than the thermal energy ($\hbar eB/m^* > kT$) the carriers are in the "quantum limit". The fields necessary to achieve this condition are also sketched in Fig. 2 using an "average" effective mass ($0.05m_0$) Shubnikov–de Hass oscillations can just be resolved in this limit.

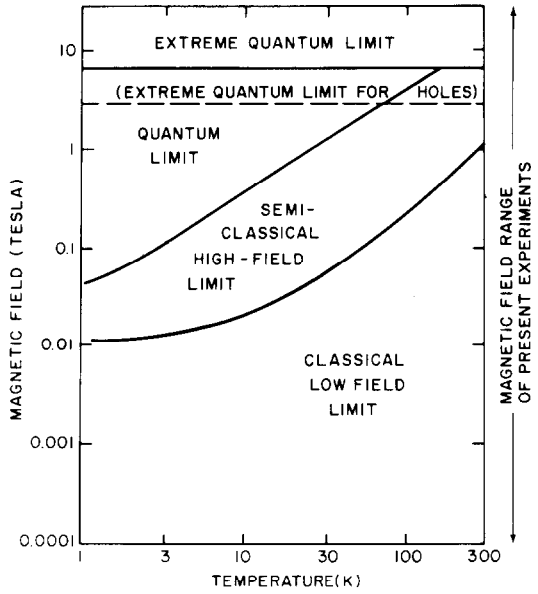

Fig. 2. Sketch showing the various magnetic fields of importance for graphite. The curves between the classical, low field, and semi-classical, low field, and semi-classical high field region are drawn for sample No. 2 of Ref. [2]. Distinctions between the various regions are not sharp and the curve is only drawn as a guide.

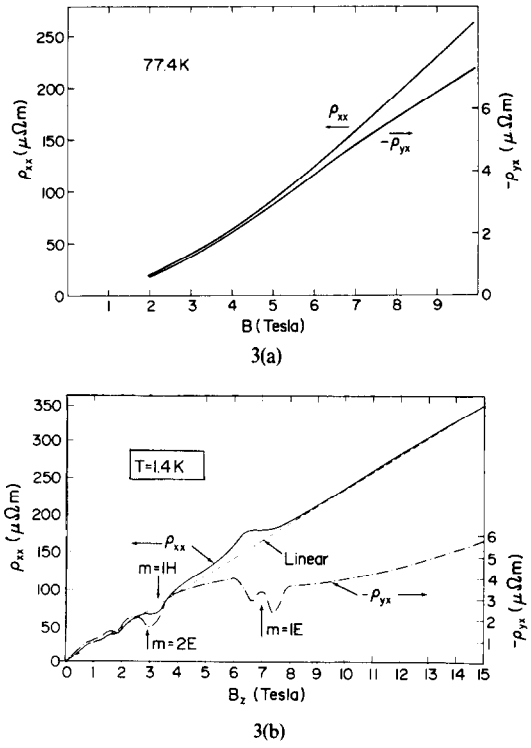

Fig. 3. Typical data for ρ_{xx} and ρ_{yx} at (a), 77.4; and (b), 1.1°K. At the upper field value, the magnetoresistance at 77.4°K amounts to $\Delta\rho/\rho_0 = 1250$ and at 1.1°K to 33,000. Shubnikov–de Haas oscillations can be seen clearly at 1.1°K. At this temperature the $m = 1$, 2 electron and $m = 1$ hole oscillations are indicated.

A third magnetic field of importance occurs when the separation between Landau levels becomes comparable to the electrochemical potential, or Fermi energy, η. Above this critical field, all of the carriers lie in *one* Landau level, the ground state level. The carriers are then said to be in the "extreme quantum limit". In graphite this occurs at about $7T$ and experiments in this region were carried out first by McClure and Spry [17]. Also indicated in Fig. 2 is the extreme quantum limit for the holes which occurs at a lower field value ($\sim 3.5T$) than for the electron states.

The extreme quantum limit field is unusually low in graphite because it is a semimetal with small Fermi energy and low carrier effective masses. By comparison the threshold field for a metal such as copper may be as high as $\sim 2\times 10^4 T$. Commercial superconducting magnetic can be purchased relatively cheaply with maximum fields $\sim 10T$, and expensively for $\sim 14T$. Facilities such as the Francis Bitter National Magnet Laboratory, Cambridge, Mass., provide steady fields up to $\sim 23T$. Thus, graphite is one material with which the quantum limit condition can be studied experimentally. It is a fascinating region in which the density of charge carriers increases linearly with field as a result of the magnetic quantization [17]. Further remarks will be made about it in Section 9.

4. THE MAGNETORESISTANCE

The simple model developed in the previous section suggested that the magnetoresistance should be proportional to B^2, provided the denominator does not deviate appreciably from unity. Using the model above ($n_1 = 1.02n_2$, $\mu_2 = 1.1\mu_1$) then the denominator only deviates from unity by 0.02% when the field reaches a value $B^* = \mu^{*-1}$, where $\mu^* = (\mu_1\mu_2)^{1/2} = (b\mu_1^2)^{1/2}$. Thus, the magnetoresistance should follow B^2 behavior well in fields less than B^*. This leads to a useful formula for estimating μ^* [12]:

$$\mu^* = \left(\frac{\Delta\rho}{\rho_0 B^2}\right)^{1/2} \text{ where } B \ll B^*. \tag{17}$$

Unfortunately, the experimental data (Fig. 3) indicate that the magnetoresistance does not follow this power law. If a plot is made of $\log \Delta\rho/\rho_0$ vs $\log B$, the slope of the line, $n(B)$, can be used conveniently to describe the field exponent of the magnetoresistance (Fig. 4).

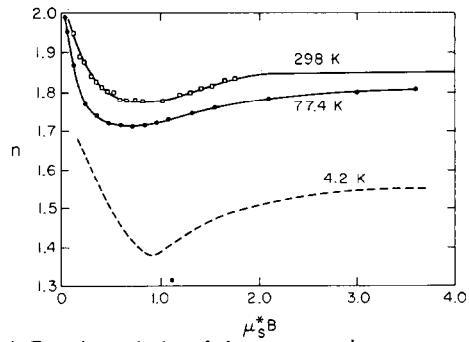

Fig. 4. Experimental plot of the magnetoresistance power law exponent, n, as a function of field at $T = 298$, 77.4 and 4.2°K [2]. Data at 4.2°K was smoothed to eliminate Shubnikov–de Haas oscillations in the magnetoresistance.

Generally the curves show dips, approaching the expected value of 2 only at very low field values ($\mu^*B \ll 1$).

At low field it is interesting to enquire whether the magnetoresistance, or other galvanomagnetic coefficients, can be universally scaled onto a single plot. The magnetoresistance of many metals can be reduced in this way onto a Kohler plot [18]. Kohler's rule needs to be modified for graphite [19] since the density of carriers changes appreciably with temperature, whereas for a metal it remains nearly constant. A suitable modification would be

$$\frac{\Delta\rho}{\rho_0} = f(\mu^*B). \tag{18}$$

A specific, possible form for the function $f(\mu^*B)$ is given in eqn (17). Unfortunately, no general function can be found to fit the data in graphite (see Fig. 4 for the different behavior of $n(\mu^*B)$ at different temperatures, for instance). This suggests that the magnetoresistance may be a very complicated phenomenon. A more detailed discussion of scaling concepts is given in Ref. [1].

As shown in Fig. 3, ρ_{xx} does not saturate at any field, and at low temperature follows a B^1 dependence closely. Also ρ_{xx} is much greater than $|\rho_{yx}|$ at high field values. It was discussed in Section 3 that the high field condition was more stringent for ρ_{xx} than σ_{xx}. Accordingly, in Fig. 5, the high field behavior of σ_{xx} is examined. A reduced logarithmic form $\sigma_{xx}(B)B/\sigma_{xx}(0)B^*$ vs μ^*B is used, where $B^* = \mu_s^{*-1}$. At high field (e.g. $B/B^* \geq 3$), the STBM indicates that the slope of this curve should be -1. As shown in Fig. 5, experimental data do not conform to this prediction. In fact at 1.1°K the curve flattens out above $\mu_s^*B = 100(B \sim 1T)$. A good test of the failure of STBM cannot be made above $\sim 3T$ since "extreme quantum limit" effects become important (Fig. 2).

Note that in the low temperature data (1.1°K) Shubnikov–de Hass oscillations can be seen. They are "washed out" at higher temperature by thermal broadening caused by collisions between carriers and lattice vibrations (phonons). Also, the oscillations are damped out by collisions between carriers and defects (e.g. dislocations, impurities, point defects, grain boundaries) and cannot be detected in highly defective samples. Note that no more oscillations are indicated above the quantum limit field ($\sim 1T$) discussed in Section 3. However, weak oscillations have been detected in this field range, to be discussed in Section 9.

In summarizing this section, the magnetoresistance is a much more complex phenomenon than is allowed for by the simple two-band model. The low-field behavior is anomalous, while at high field the semi-classical prediction for its field dependence is not obeyed. The magnetoresistance can still be useful as a tool for characterising specimens, as will be discussed in Section 6. Shubnikov–de Haas oscillations can be useful in some cases for characterising neutron-irradiated specimens, as discussed in Section 8. The quantum limit is currently being studied, and a brief description of our work is given in Section 9.

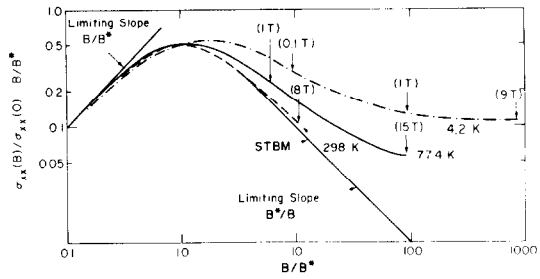

Fig. 5. Plot of $\sigma_{xx}(B) \cdot B/\sigma_{xx}(0) \cdot B^*$ vs B/B^* at 298, 77.4 and 1.1°K. At 77.4 and 1.1°K the data are derived from that in Fig. 5 with Shubnikov–de Haas oscillations smoothed from data at 1.1°K. The curve for STBM is drawn with $n_1 = 1.02n_2$, $\mu_2 = 1.1\mu_1$.

5. THE HALL EFFECT

The Hall Effect is much more difficult to understand than the magnetoresistance because contributions from carriers of different sign (electrons and holes) are subtractive, rather than additive, as in the magnetoresistance. At low field the Hall coefficient or ρ_{yx} can change sign even for a simple two band model (Fig. 1). Typical data for ρ_{yx} over a wide field range are shown in Fig. 3.

At low field, however, the variation of the Hall coefficient is complicated and cannot be fitted by a two-band model. Note the unusual changes that occur in $R_H(B)$ at very low field, as indicated in Fig. 6. A negative-going spike is invariably seen in HOPG. Cooper *et al.* [20] found that, upon further annealing, the behavior at 77°K was characterised by a positive-going trend similar to that seen by Soule [12] in SCG at the same temperature (Fig. 6). Note, however, that the same sample of SCG shows a negative-going trend at low field at 4.2°K (Fig. 6). Samples of Kish graphite with high perfection (see Section 6) appear to show negative-going trends at low field [13, 21].

Soule [12] originally interpreted the positive-going trend at 77°K in terms of a mobile, minority hole. Pockets of light holes are located in the corners of the Brillouin zone. However, all the low field trends in $R_H(B)$ cannot be related to these carriers, since in most specimens the Hall behavior is electron-like (negative trend).

Experimentally, $|\rho_{yx}|$ is always much smaller than ρ_{xx}. This is related to the anomalous field-dependence of ρ_{xx} and σ_{xx} discussed in the previous section. The sign of the charge carrier with the higher density can be inferred from the sign of the Hall coefficient at high field, but because $|\rho_{yx}| < \rho_{xx}$ at all fields the high field limit equation (16) cannot be used. Instead, the limiting equation for σ_{xy} (eqn 14) may be used, since this conductivity component tends to B^{-1} dependence as predicted by general, semi-classical models.

It is interesting to note that the difference in carrier densities $(N-P)$ where N is the total electron, and P the hole densities, is usually smaller for high quality samples of HOPG ($\sim 0.4 \times 10^{22}\,m^{-3}$ using data from Fig. 3 at 1.1°K) than SCG ($\sim 1.5 \times 10^{22}\,m^{-3}$)[22]. In this one respect HOPG is more "perfect" than SCG. A further discussion of the relationship between galvanomagnetic

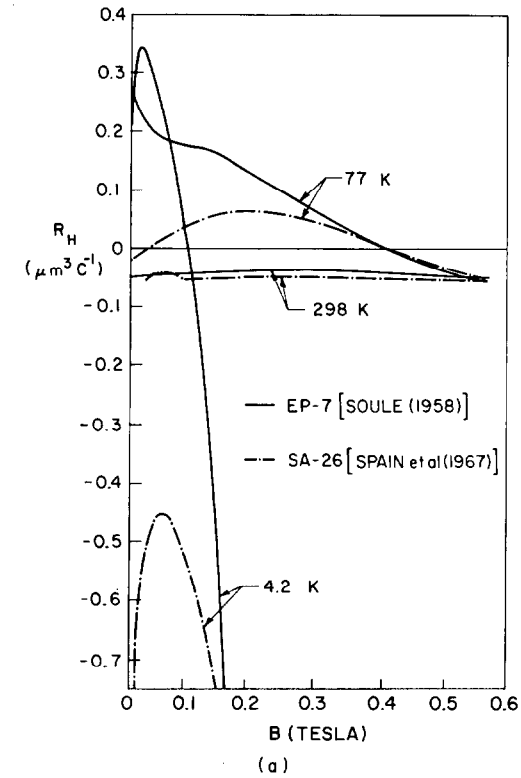

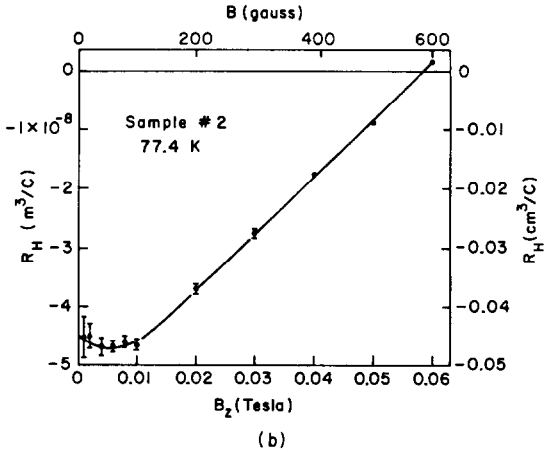

Fig. 6. (a), Hall effect data for HOPG [13] and SCG [11] below $0.6T$. More detailed measurements for HOPG can be found in Ref. [2]. Note the trends at very low field. (b), Detail of curve at 77.4°K, $B < 0.06T$ [2].

properties and sample perfection is given in Section 6.

In summary, the Hall coefficient is anomalous at low fields. Results show that samples of SCG, HOPG and Kish graphite are nearly compensated ($(P-N) \ll P, N$). Furthermore, the mean carrier mobilities of electrons and holes are roughly equal. Although the high field asymptote of R_H cannot be used to estimate $(P-N)$ reliably, because of the anomalous behavior of ρ_{xx}, $\sigma_{yx}B$ behaves semi-classically at high field, suggesting that $(P-N)$ may be obtained from its asymptotic value.

6. THE MOBILITY OF THE CHARGE CARRIERS

It is of interest to evaluate the mean mobilities for the charge carriers from galvanomagnetic data. As outlined in eqn (6) the mean free path may then be obtained. At $T = 0$°K, all carrier scattering results from defects, so that valuable information can be gained about the density of defects. Measurements need not be carried out at very low temperature, since the relaxation times due to defects and intrinsic scattering mechanisms can be summed using Mathiesson's rule [17]. In practice, 77°K (liquid nitrogen temperature) is a useful measurement temperature. Several different methods for evaluating mobility are summarised in Table 1, and discussed below.

6.1 *Mean conductivity mobility*

A mean conductivity mobility can be defined from eqn (7) in which n is the total number of carriers $(N + P)$.

$$\sigma_{xx}(0) = \rho_{xx}^{-1}(0) = (N + P)e\langle\mu_c\rangle. \tag{19}$$

Values of $(N + P)$ used here were calculated by Prof. McClure, using band parameters in SWMcC discussed in Ref. [11]. Data for $\langle\mu_c\rangle$ are illustrated in Fig. 7 for HOPG [2]. Although the above value of mobility, which is an arithmetic mean of μ_1 and μ_2 for the two-band model, is useful, it is convenient to have a measure of mobility without recourse to a calculation of the density of carriers. In principle this can be obtained from the magnetoresistance or magnetoconductivity.

6.2 *Magnetoresistance mobility due to Soule, μ_B^**

Soule [12] proposed the use of eqn (17) for the mobility. Realizing that it only represented a rough guide to the mobility, he suggested that it would be convenient to measure it at a fixed field, which he chose to be $0.3T$.

$$\mu_B^* = \left(\frac{\Delta\rho}{\rho_0 B^2}\right)^{1/2}_{B=\text{constant}} \tag{20a}$$

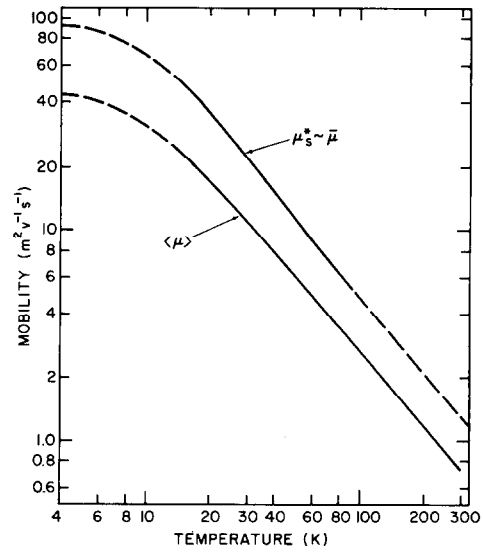

Fig. 7. Comparison of the scaled magnetoresistance mobility, μ_s^*, in eqn (20b), or magnetoconductivity mobility, $\bar{\mu}$, in eqn (22) as a function of temperature, compared to the average drift mobility $\langle\mu\rangle$, in eqn (19).

Table 1. Mobilities discussed in present paper

Symbol	Definition	Name	General remarks	Value† ($m^2v^{-1}s^{-1}$)
μ^*	$\left(\frac{\Delta\rho}{\rho_0 B^2}\right)^{1/2}$	Magnetoresistance mobility	Value not defined unless magnetic field specified	—
μ_B^*	$\left(\frac{\Delta\rho}{\rho_0 B^2}\right)^{1/2}_{B=\text{const.}}$	Magnetoresistance mobility	Magnetic field specified for all temperatures usually chosen as $0.3T$	43.2 ($B = 0.3T$)
μ_s^*	$\left(\frac{\Delta\rho}{\rho_0 B^2}\right)_{\mu^* B=1}$	Scaled magneto-resistance mobility	The value of reduced field at which value is calculated can take other values than $\mu_s^* B = 1$	91.1
μ^+	See eqn (21) in text	Mobility of Kawamura *et al.* [13]	Based on simplified two-band model. Value depends on field range over which data taken.	45.6 (data to $0.3T$) 37 (data to $2T$) ~ 90 (data to 0.01T)
$\bar{\mu}$	$\bar{\mu} = B_{1/2}^{-1}$ (see eqn 22)	Scaled magneto-conductivity mobility	Definition can be generalized (see Ref. [1])	93.3
$\langle\mu_c\rangle$	$\frac{\sigma_{XX}(0)}{\lvert e\rvert(N+P)}$	Conductivity mobility	Mobility in principle gives "best" mobility, but depends on knowledge of $(N+P)$	44.4

†Based on sample No. 2 of HOPG of Ref. [2] at 4.3°K. $\sigma_{XX}(0) = 36.0 \times 10^6(\Omega\text{m})^{-1}$, $(N+P) = 5.7 \times 10^{24}\text{m}^{-3}$: $\rho_{300°K}/\rho_{4.2°K} = 14.5$.

The main difficulty with the use of (17) is that values of mobility depend on the value of magnetic field. Typical curves of $\mu^*(B)$ are given in Fig. 8 for HOPG. If the magnetic field is fixed at some arbitrary value, the resulting curve $\mu_B^*(T)$ will necessarily give values which are relatively reduced at lower temperature, and relatively increased at higher temperature. This difficulty can be overcome through the use of scaling concepts, to be discussed later.

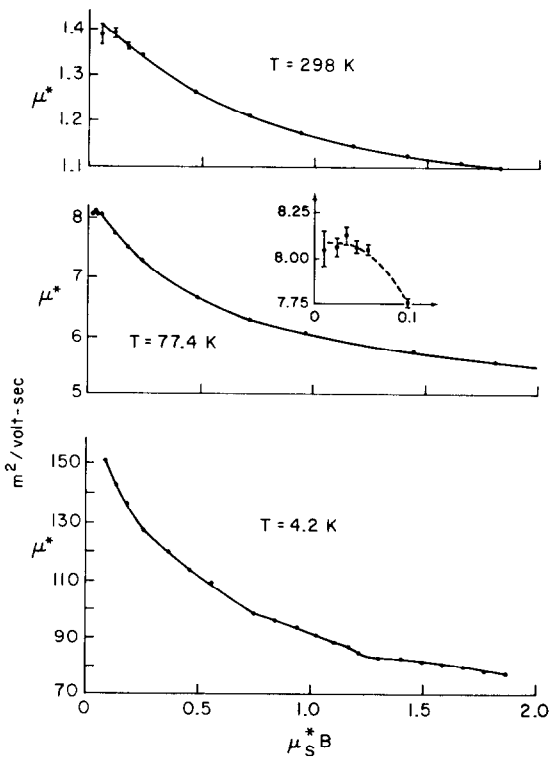

Fig. 8. The magnetoresistance mobility from eqn (17) plotted as a function of reduced field, μ_s^*, at 298, 77.4 and 4.2°K. μ^* and μ_s^* are defined in the text and Table 1.

6.3 *Mobilities based on two-band analysis of galvanomagnetic data*

If the curves of $\rho_{xx}(B)$ and $\rho_{yx}(B)$, or $\sigma_{xx}(B)$ and $\sigma_{xy}(B)$ can be fitted with a two-band model, using formulae such as (10a) and (10b), etc. then mobilities μ_1 and μ_2 can be obtained directly. However, the data cannot be fitted well in this way, even using multiple carrier models, as originally indicated by McClure [8]. Specific difficulties such as anomalous low and higher field behavior have already been discussed.

Kawamura *et al.* [13] proposed a method based on a simplified form of the two-band formula for the magnetoresistance (11):

$$\frac{B^2}{\Delta\rho/\rho_0} = \mu^{+2} + \left(\frac{N-P}{N+P}\right)^2 B^2. \tag{21}$$

Thus, a plot of $B^2/\Delta\rho/\rho_0$ V B^2 should yield a straight line with intercept μ^{+2}. The experimental data for HOPG do not give a straight line for any part of this plot (Fig. 9). Furthermore, published data on $\Delta\rho(B)/\rho_0$ for Kish graphite indicate a similar form to HOPG. A two-band model is *not* expected to fit the data and the method of Kawamura *et al.* will give an intercept which depends on the field range over which the data is taken (see Fig. 9). Kawamura *et al.* [13] take measurements to $0.6T$, and use an approximately linear portion of their curve between 0.35–$0.6T$. However, if data are taken to higher field, then a different intercept can be obtained, as shown in Fig. 9. Resulting mobility values for a sample of HOPG are listed in Table 1.

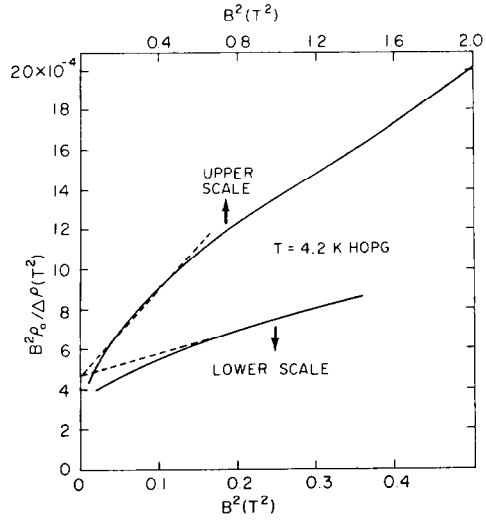

Fig. 9. A plot of $B^2\rho_0/\Delta\rho$ vs B^2 for HOPG [2] as proposed by Kawamura *et al.* [13]. The lower curve is drawn approximately to the same scale and field range as in Ref. [13]. The upper curve extends data from the same specimen to higher field values. The dashed line is the same in each case, indicating that the portion of the lower curve which appears as a straight line is in fact part of a curve.

6.4 *Mobility values based on scaling concepts*

As discussed earlier, magnetoresistance data obtained at different temperatures cannot be scaled onto a universal curve (eqn 18). However, a scaled mobility value can be obtained if magnetoresistance or magnetoconductivity formulae are used at the same value of reduced field at all temperatures. For the scaled magnetoresistance mobility, μ_s^*:

$$\mu_s^* = \left(\frac{\Delta\rho}{\rho_0 B^2}\right)^{1/2}_{\mu_s^* B = \text{constant}}. \tag{20b}$$

It is proposed that the specific value of $\mu_s^* B$ be chosen as unity [1]. At this field, anomalous effects from trigonal warping should be minimized [3] while field values should not be too high that linear magnetoresistance anomalies or quantum effects (Fig. 2) are important. The value $\mu_s^* = 1$ is therefore a compromise.

A similar scaled mobility based on the conductivity component σ_{xx} is:

$$\bar{\mu} = B_{1/2}^{-1} \tag{22a}$$

where

$$\sigma_{xx}(B_{1/2}) = \tfrac{1}{2}\sigma_{xx}(0). \tag{22b}$$

The definition can be generalized, as discussed in Ref. [1]. Although this formula is more firmly based on theoretical grounds than (20), the two scaled mobilities μ_s^* and $\bar{\mu}$ differ by less than about 2% for typical materials (Table 1). The difference is too small to be of much consequence and will be ignored in this paper.

6.5 *Comparison of mobility values*

All of the above prescriptions give different values for the mobility. To illustrate the differences, the mobilities have been calculated for a sample of HOPG at 4.2°K (sample No. 2 of Ref. [2]) and are recorded in Table 1. If the magnetoresistance could be explained on the basis of a two-band model, then all of the mobilities in Table 1 would lie within a few per cent of each other. If the density of carriers calculated by McClure is correct, then $\langle\mu_c\rangle$ must represent the "best" value of the mean mobility. One aim of any theoretical model for the galvanomagnetic properties of graphite should be an understanding of the reasons for the discrepancy between these values.

If $\langle\mu_c\rangle$ represents the "best" value for the mobility, then Kawamura *et al.*'s [13] value at 4.2°K is the "nearest" obtained from the magnetoresistance. However, this is accidental, since it results from the arbitrary field range over which they took data, dictated by the limitations of the magnet used for the measurements. With another magnet or at another temperature, their value of mobility could have been "worse" than other values.

In the next section results of some theoretical models will be presented, which allow some of the anomalies discussed above to be understood. These models cannot explain the reason for the large ($\sim \times 2$) difference between $\langle\mu_c\rangle$ and μ_s^* or $\bar{\mu}$. In the absence of a satisfactory explanation, it is suggested that experimental results for mobility should be expressed in terms of μ_s^* or $\bar{\mu}$. Between about 77 and 300°K, μ_B^* measured at $0.3T$ is an acceptable alternative, because it is based on experimental convenience.

6.6 *Use of mobility values for assessing specimen perfection*

In spite of the fact that estimates of mobility are anomalously high, differences in mobility for different specimens have been used to assess material perfection [14, 23–27]. The mobility at low temperature is a blunt tool for this purpose since it only gives a measure of the weighted separation of defects responsible for scattering. It cannot distinguish between different defects and may be relatively insensitive to certain types of defects, e.g. neutral substitutional impurities.

The resistivity ratio of metals between 300 and 4°K is often used as an indication of specimen quality. Essentially this ratio is the mobility ratio, since the density of carriers is independent of temperature for a good metal. For graphite the density of free carriers increase about four-fold between 4 and 300°K, so that the resistivity ratio and mobility ratio differ by this factor. Also, acceptor or donor-type defects may change the density of free carriers, since graphite is a semimetal with only one free carrier for $\sim 10^4$ atoms.

In a sample of HOPG with very large basal crystallite dimension ($\sim 4\mu$m) the resistivity ratio may approach $\rho_{300°K}/\rho_{4°K} \leq 20$, corresponding to a mobility ratio $\sim 80(\mu_s^*(4°K) \sim 100\ \text{m}^2\text{v}^{-1}\text{s}^{-1}$, $\mu_s^*(300°K) \sim 1.25\ \text{m}^2\text{v}^{-1}\text{s}^{-1})$. Purified natural crystals have been studied with resistivity and mobility ratios about twice these values [12], and slightly higher ratios have been found recently for Kish graphite [13]. More typical values for HOPG or PG are

$(\rho(300°K)/\rho(4°K) \sim 4;$ $\mu_s^*(4°K) \sim 18\ m^2v^{-1}s^{-1};$ $\mu_s^*(300°K) \sim 1.1\ m^2v^{-1}s^{-1})$. It is to be noted that the resistivity and mobility at, or near 300°K are not changed appreciably, until the resistivity ratio falls to about unity, because electron-phonon scattering predominates. However, trends in the mobility at liquid nitrogen temperature (77°K) can be used as a convenient measure of sample perfection without the expense and equipment complication of liquid helium.

The idea of using resistivity ratios and mobilities to assess defects in highly graphitized materials is certainly not new. Earlier work has been carried out in several laboratories [14, 23–27]. However, more recent work on galvanomagnetic properties has refined the definition of mobility and its interpretation in terms of scattering phenomena. This will be addressed in the following section.

7. GALVANOMAGNETIC EFFECTS AND THE ELECTRONIC STRUCTURE OF GRAPHITE

In the previous sections certain problems with the interpretation of galvanomagnetic data were discussed. In this section more detailed calculations will be considered which will help to explain some of the anomalous behavior. A complete understanding is not possible at the present time, but the calculations have illustrated some of the complexities and subtleties of the transport properties of graphite.

Compared with the simple two-band model, the actual electronic properties of graphite differ in three major ways:

(1) In STBM all carriers within a band have the same effective mass and relaxation time. In SWMcC the effective mass varies markedly along the edge of the Brillouin zone. The relaxation time is also expected to vary (see later discussion). In effect, the properties should be described by a Multiple-Carrier-Group-Model (MCGM), in which a thin slice of carriers within the element of k-space k_z to $k_z + \Delta k_z$ is considered to have the same effective mass and relaxation time.

(2) Within such a slice the constant energy surfaces are not circular, but have three-fold warping. The degree of warping varies along the zone edge, roughly diminishing from the centre of the zone edge to the zone corners where the surfaces are circular. In the region between electrons and holes, the trigonal warping produces off-edge connecting arms. Transport effects are strongly affected by the warping.

(3) In the formulae for STBM, the mobilities used in expressions for σ_{xx} (conductivity mobility) and σ_{xy} (Hall mobility) were the same. This is strictly true only for very low temperature ($kT \ll \eta$, where k is Boltzmann's constant, T the absolute temperature, η the electrochemical potential or Fermi energy). This is called the region of degenerate statistics. At ambient temperature, $kT/\eta \sim 1$, so that non-degenerate statistics are applicable, and the Hall and conductivity mobilities are not identical.

Calculations have been made to assess the effects of these three factors on the galvanomagnetic coefficients. The effects of carrier non-degeneracy are not as important as the other two factors, and experiments show that anomalies tend to be less pronounced at higher temperature. Further discussion of carrier non-degeneracy is left to Ref. [2].

Figures 10 and 11 indicate the effect of the variation of mobility along the zone edge (MCGM) on the conductivity components σ_{xx}. Two models of the relaxation time have been used in these figures: (a) Mean free path, λ = constant; (b) Relaxation time, τ = constant. At low-field (Fig. 10) the reduced conductivity is depressed below the simple case, but at high-field (Fig. 11) the reverse is true. However, the model does not explain the anomalous high-field behavior for $B/B_{1/2} \gtrsim 10$, nor can it explain the low-field anomalies in the Hall effect.

The complexity introduced by trigonal warping can be illustrated by simplifying the shape of the constant energy surfaces as shown in Fig. 12 by arcs of circles. For the purpose of calculation, the transport properties can be calculated by rearranging these segments into two separate circles. Considering the electrons, the small

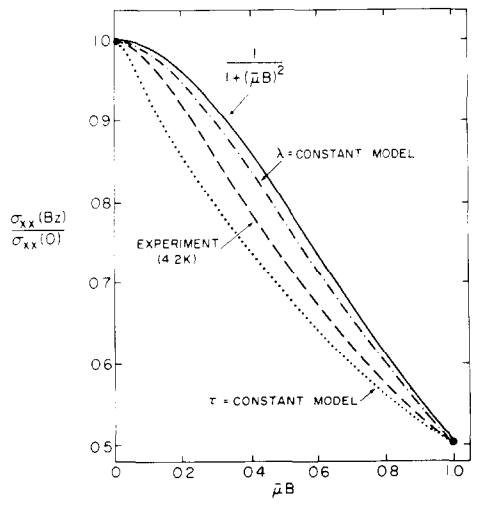

Fig. 10. A reduced plot of $\sigma_{xx}(B)/\sigma_{xx}(0)$ vs $B/B_{1/2}$ in the low field region for STBM, MCGM (constant relaxation time) and MCGM (constant mean free path) compared to experimental data at 4.2°K.

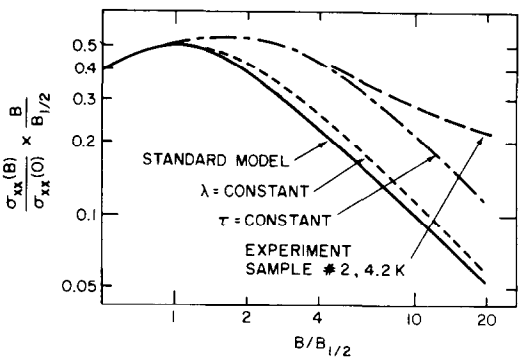

Fig. 11. A reduced plot $\sigma_{xx}(B) \cdot B/\sigma_{xx}(0)B_{1/2}$ vs $B/B_{1/2}$ for STBM and MCGM compared to experimental data. Note that the constant relaxation time model fits the data well up to $B/B_{1/2}$ 4. At higher field the calculation gives a slope of $-1(\sigma_{xx}\alpha B^{-2})$ while the experimental data tend to saturate $(\sigma_{xx}\alpha B^{-1})$.

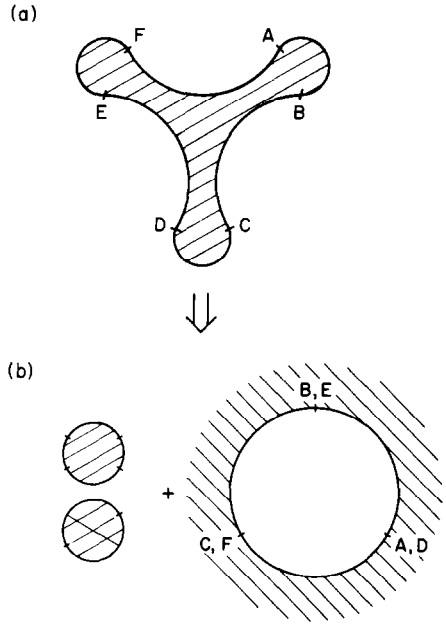

Fig. 12. (a), Simplified form for the trigonally warped electron Fermi surface in graphite. (b), The same surface reconstructed into equivalent electron and hole surfaces. Shaded areas represent filled states.

circle resulting from the tips of the trigonally-warped surface is electron-like, since states with lower energy lie inside the circle. However, the larger circle is *hole*-like since states with lower energy lie outside the circle. Thus, for this simplified form of the trigonally-warped surface, the properties of a thin slice of electrons can be represented by a group of electrons plus a larger group of holes. Because the electron circle is smaller, these carriers dominate at low field (they turn through larger Hall angles). At higher field the hole carriers dominate. Finally, calculations show that at very high field σ_{xy} tends to the semi-classical limit given earlier.

For SWMcC the segments of the constant energy surfaces are not arcs of circles and the velocity of the carriers has to be Fourier-analysed. The result of a model calculation (6) is shown in Fig. 13 in which the ratio of σ_{xy} calculated for the trigonally warped surfaces is compared to that of unwarped (circular) surfaces. The sharp dip occurs when the carriers in segments with negative curvature predominate. Over a region of magnetic field the electron states may behave as holes in the Hall effect, and vice-versa!

Similar calculations for σ_{xx} using this Model (3) show that trigonal warping is very important at lower fields (e.g. $B/B_{1/2} < 1$)(Fig. 14). The variation of $\sigma_{xx}(B)$ is similar to that for MCGM illustrated in Figs. 10 and 11. In both cases a minimum occurs in the magnetoresistance power-law exponent, n, with field, similar to that obtained experimentally (Fig. 4). This is not surprising, since in both MCGM and calculations using trigonally-warped surfaces, a range of values of mobility is introduced for each carrier (mobility dispersion). At zero field the conductivity can be increased by a factor of ~ 1.5 over that obtained for a model with the same relaxation

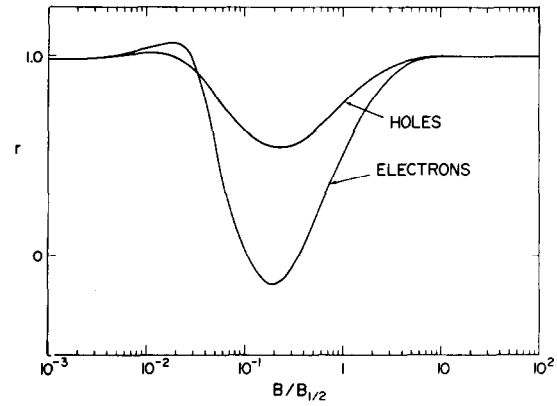

Fig. 13. A possible variation for the ratio of the Hall conductivity $\sigma^t_{xy}/\sigma^c_{xy} = r$, where t represents the calculation for the trigonally warped surface and c for a pocket with the same number of carriers, but circular cross-sections.

time, but constant energy surfaces with circular cross-section. Apart from being important in the magnetic field dependence of σ_{xx}, trigonal warping is also important in the pressure dependence of the conductivity [29].

The calculations are very lengthy, even for simplified models of the constant energy surfaces and relaxation time. A quantitative fit to the Hall and magnetoresistance data has not been made, but it is believed that anomalies at low field can be explained in this way. The difficulty of using Hall and magnetoresistance data to obtain carrier densities and mobilities is apparent. Although estimates can be made using simple models, such as STBM, the values derived may be misleading. Trends of properties with specimen perfection may be interpreted much more readily, but caution should be exercised.

In the above calculations, very crude approximations

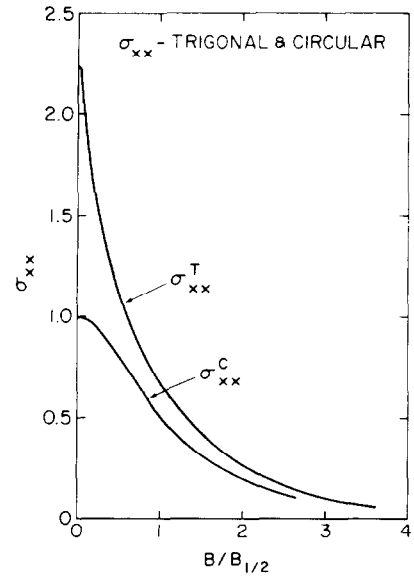

Fig. 14. A plot of $\sigma_{xx}(B)$ for electrons in a trigonally warped surface (SWMcC) compared with that for the same number of electrons in a pocket with circular cross-section with the same relaxation time τ. Note the enhancement of σ_{xx} due to trigonal warping.

for the relaxation time were used. At the same time, detailed models of the constant energy surfaces, effective masses, etc. can be used. This is clearly an undesirable situation. Scattering processes are extremely complex in graphite, so that very little progress is expected in our *quantitative* understanding of low-field properties.

At higher field (e.g. $\mu^* B \geq 4$, but B well below the quantum limit) the conductivity component σ_{xx} should decrease as B^{-2}, even for complex models of the dispersion relationship. Experimentally, this was not observed, and the reason is not understood. In fields above $\sim 1.5T$ the density of carriers begins to increase, becoming roughly linear above the quantum limit field ($\sim 7T$). Even when allowance is made for this in interpreting σ_{xx} and ρ_{xx}, non-classical behavior is observed. It is possible that the scattering processes are dependent on magnetic field, or that quantum effects produce a non-quadratic dependence.

At the present time it has not been possible to reconcile the difference between the conductivity mobility, $\langle \mu_c \rangle$ and the magnetoresistance mobility, μ_s^*, or magnetoconductivity mobility, $\bar{\mu}$. Although either the MCGM or trigonal warping models introduce important modifications to the low field behavior, the average mobilities calculated from $\rho_{xx}(B)$ or $\sigma_{xx}(B)$ do not differ by more than about 15% from the conductivity mobility. It is extremely unlikely that more detailed models of the relaxation time can help to explain the observed difference of about a factor of two ($\mu_s^* \sim \bar{\mu} \sim 2\langle \mu_c \rangle$).

It appears that there is a basic problem with our understanding of the transport properties which requires careful consideration. The simplest explanation is that the number of carriers calculated from the Slonczewski Weiss model is in error by a factor of about two. However, this requires a complete re-examination of all the band parameters in SWMcC, and many experiments can be fitted satisfactorily to the present model. A satisfactory explanation of the present problem with both the mobility values and the field dependence of σ_{xx} awaits further developments.

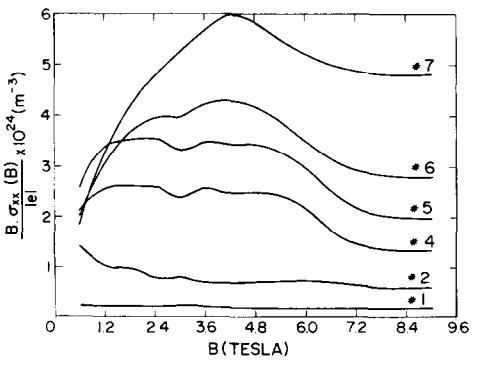

Fig. 15. Variation of $\sigma_{xx}B$ with field for samples irradiated to different dose levels. Note that $\sigma_{xx}B$ tends to a constant value at high field. Data are taken at ~ 1.4°K. Dose levels for each sample # are given in Table 1.

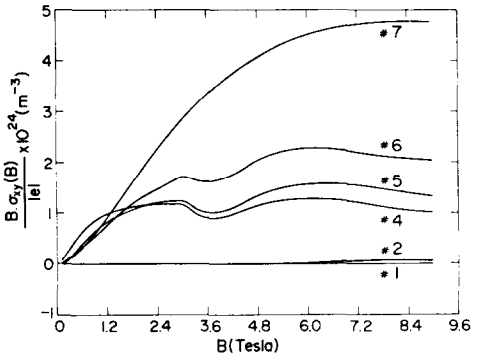

Fig. 16. Variation of $\sigma_{xy}B$ with field for samples irradiated to different dose levels. $\sigma_{xy}B$ tends to a constant value. Data are taken at ~ 1.4°K.

8. THE EFFECT OF NEUTRON IRRADIATION ON THE QUANTUM LIMIT GALVANOMAGNETIC EFFECTS

Samples of HOPG have been irradiated with fast neutrons to doses in the range 0.18–2.9×10^{17} nvt ($E >$ 1 MeV). ρ_{xx} and ρ_{yx} were then measured to $\sim 9T$. By this field both $\sigma_{xx}B$ and $\sigma_{xy}B$ were found to reach approximately constant values (Figs. 15 and 16). Values for the acceptor density. $(P - N)$ were obtained from the limiting value of σ_{xy}. B, as suggested by eqn (14). By plotting $\sigma_{xy}B/|e|$ in Fig. 15, acceptor densities can be read directly off the graph.

Fast neutron irradiation knocks atoms out of lattice sites into interstitial positions. At 90°C, the temperature of irradiation, some annealing has already taken place, and interstitial atoms will have diffused into interstitial loops (for a review, see Ref. [30]). There are many studies in the literature which discuss changes in electronic properties of polycrystalline graphite. The results are qualitatively similar to those in PG [31], where the Hall coefficient becomes more positive with irradiation, the resistivity is increased, and the magnetoresistance lowered. Acceptors are presumably related to the formation of vacancies, although this is not established definitely.

As discussed in Sections 3 and 5, the acceptor concentration may not be obtained from the limiting value of the Hall coefficient, because use of the field limit formula (16) assumes that $\rho_{xx} \ll |\rho_{yx}|$. In all samples studied, $|\rho_{yx}| < \rho_{xx}$ at all fields (compared Figs. 15 and 16). This is the first study to have attempted to find acceptor concentrations at high field, and the only study to use the asymptotic value of $\sigma_{xy}B$. It is emphasized that eqn (14) is *assumed* to hold, since $\sigma_{xy}B$ follows the semiclassical predictions. However, the anomalous behavior of $\sigma_{xx}(\sigma_{xx}B$ saturates (Fig. 15) rather than $\sigma_{xx}B^2)$ is troublesome, since it shows that galvanomagnetic effects are not understood in this field range.

Values for the rate of acceptor production per unit radiation dose are listed in Table 2. Values are given on the basis of eqn (14) for doses measured on the basis of two energy criteria (> 0.1 MeV, > 1 MeV). Also, for comparison, the value is also given for the same data using Hall data alone (ρ_{yx}) and eqn (16). The much higher value obtained by Blackman *et al.* [31] is related partially

Table 2. Comparison of values for the rate of production of acceptors with neutron dose level

Reference	Type of measurement	Acceptor rate (ppm/10^{17} nvt)	Comment
Blackman *et al.* [31]	Hall effect ($B \leq 0.5T$) ($T \sim 295$°K) (eqn 16)	~75	$E > 1$ MeV
Cooper *et al.* [32]	Shubnikov de Haas ($T \sim 1$–4°K)	2.8	energy criterion not given
McClure [33]†	magnetic sucepti-bility, ESR and Hall data	5.7	$E > 0.25$ MeV
Present results	galvanomagnetic data 4.2°K, $8T$(eqn 14)	(14 ± 3)	$E > 1$ MeV
		(9 ± 2)	$E > 0.1$ MeV
	4.2°K $8T$(eqn 16)	(30 ± 10)	$E > 1$ MeV

†Similar results have been found by Wagoner, based on analysis of galvanomagnetic, ESR and magnetic susceptibility measurements (G. Wagoner, private communication, 1977).

to their use of eqn (16), and also to use of Hall data at low field ($\leq 0.6T$). A much lower value was obtained by Cooper *er al.* [32] in which acceptor levels were inferred from changes in Shubnikov–de Hass frequencies. The shifts in the frequencies were small, and complicated fitting proceedures were necessary to derive the shifts. An intermediate value was reported by McClure [33], who analysed a number of experiments. The discrepancy between the present values and his is not clear.

The data were also of interest since shifts of the extreme quantum limit Shubnikov–de Haas oscillations could be measured with irradiation. Extrema in ρ_{xx} and ρ_{yx} occur whenever maxima or minima with respect to k_z of magnetic energy levels are in coincidence with the Fermi level. The calculated values of field at which the $m = 1$, 2 electron and $m = 1$ hole quantum levels are in this coincidence condition are plotted in Fig. 17 as a function of acceptor concentration.

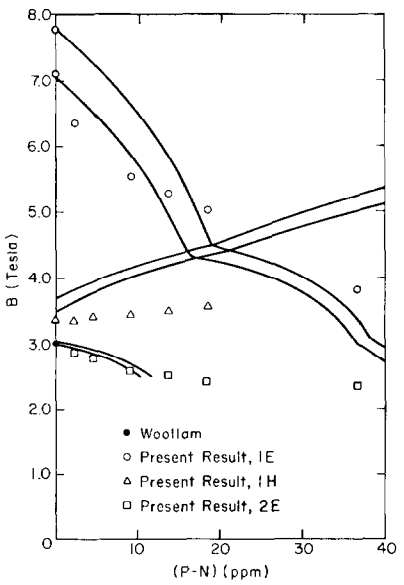

Fig. 17. The variation of the coincidence fields with acceptor concentration for the $m = 1$, 2 electron, and $m = 1$ hole magnetic quantum levels. The full line is the result of rigid-band theory, including spin splitting. Results of experiment are indicated by circles and represent positions of extrema in $\rho_{xx}(B)$ and $\rho_{yx}(B)$ data. Apart from the unirradiated sample, spin splitting could not be resolved in the experiments.

The model assumes that the only effect of the acceptors is to lower the Fermi energy, with all other band parameters held constant (rigid band model). Since the lattice parameters vary by less than 0.2% in the dose range examined, this was thought to be a reasonable approximation.

Experimentally the coincidence fields are associated with extrema in $\rho_{xx}(B)$ and $\rho_{yx}(B)$ as indicated for the magnetic levels of interest in Fig. 3(b) for unirradiated graphite. Allowance must be made for the fact that the position of the extrema in ρ_{xx} or ρ_{yx} can be shifted by electron scattering. Thus, in Fig. 17, the shifts in extrema recorded between the most lightly irradiated specimen, No. 2, and the irradiated specimen, No. 1, were probably due to the increased scattering.

The following conclusions may be drawn from these results.

(1) The downward shift of electron, and upward shifts of hole extrema in ρ_{xx} and ρ_{yx} are in agreement with the assignment of electrons near the centre of the Brillouin zone edge. This corresponds to a negative value of the band parameter γ_2. The shifts of low field Shubnikov–de Haas frequencies of neutron-irradiated graphite were also consistent with this carrier assignment, which has been the subject of several studies over the last few years (see Ref. [34] and discussion in Ref. [35]). Soules' results on boron-doped graphite [36] are the only ones that are apparently consistent with a *positive* value of γ_2.

(2) Although downward shifts of the electron extrema are in rough agreement with the calculated values, the upward shift of the hole, $m = 1$, extremum is too small to be accounted for on the basis of the rigid band model. Cooper *et al.*'s results [32] suggested this also, but scatter was too high to enable definite conclusions to be reached [10]. Attempts were made to determine changes that could occur in band parameters in SWMcC, but the data could *not* be fitted with reasonable changes. This awaits a satisfactory explanation.

A comprehensive account of this work can be found in Ref. [4].

9. GALVANOMAGNETIC EFFECTS IN THE QUANTUM LIMIT

In the quantum limit it is of interest to compare the experimental variation of σ_{xx} and σ_{xy} with calculated behavior. McClure and Spry [19] predicted that $\sigma_{xx}B$ and $\sigma_{xy}B$ should be constant in this field region for a sample in which ionised impurity scattering predominated, and this behavior was approximately observed in their SCG samples. Woollam [37] later found non-linear behavior in σ_{xx} for SCG up to $\sim 20T$.

Data for HOPG have been reported at 298, 77, 4.2 and 1.1°K by us, up to $23T$ [5, 38]. Representative curves of $\sigma_{xx}B$ and $\sigma_{xy}B$ are shown in Figs. 18 and 19. Neither of these quantities is constant at any temperature for this material.

An interesting observation is that the curves do not vary smoothly, but have small "bumps." Shubnikov–de Haas oscillations are not expected in this field range (a further Shubnikov–de Haas oscillation is expected in excess of $50T$ due to splitting of the ground state energy level). Further work is necessary to establish more clearly whether or not the effects are intrinsic. However, they have been observed in two samples, and oscillations have also been seen in c-axis magnetoresistance of two samples. A possible explanation is that they are magneto-phonon oscillations, but further work is required to establish this conjecture.

10. CONCLUSIONS

In spite of the large number of publications which have considered galvanomagnetic properties of graphite, there are many problems which remain to be solved before a quantitative understanding is reached. However, it is important that these properties are well understood before galvanomagnetic properties are used to characterize changes that occur with specimen perfection, doping, or formation of dilute lamellar compounds. In some cases these properties are the only ones that can be measured conveniently.

In the preceeding sections some advances in our understanding have been outlined. Complexity in these properties is now qualitatively understood. The inadequacy of the simple two-band model (STBM) has been clearly demonstrated. This work illustrates the difficulty of quantitatively determining carrier mobilities and densities from magnetoresistance and Hall data. However, trends in properties can be used to assess *changes* in scattering of carriers and acceptor or donor concentrations.

A major problem still remains with the anomalous behavior of σ_{xx} in fields which are lower than the extreme quantum limit, but for which $\mu^*B \gg 1$. At the present time a qualitative understanding of this is not even available. (The anomalous maximum in the high field resistivity observed by Kreps and Woollam [39] and Ayache and de Combarieu [40] may be related to this problem.) A fundamental problem remains with the lack of agreement between the conductivity and magneto-conductivity mobility. In the quantum limit more refined calculations are required to understand the field dependence of σ_{xx} and σ_{xy}. Also the origin of the weak oscillations (whether intrinsic or extrinsic) needs to be examined.

Acknowledgements—Particular thanks are due to Dr. R. O. Dillon, Dr. W. H. Lowrey, Prof. J. W. McClure and Dr. J. A. Woollam, who have colaborated in various aspects of this study.

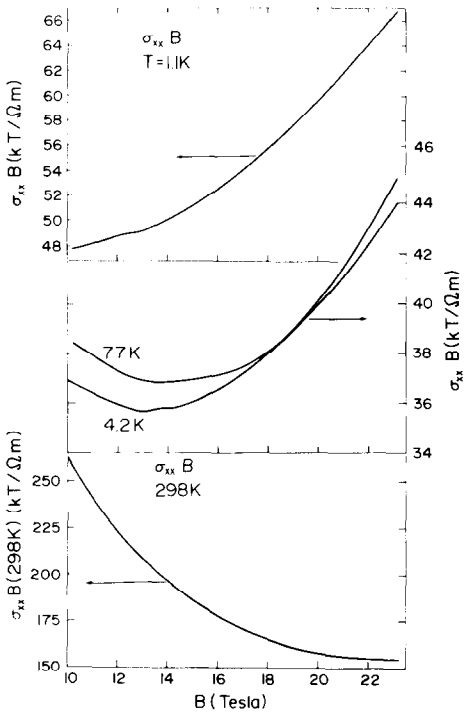

Fig. 18. Curves of $\sigma_{xx}B$ vs B in the quantum limit for HOPG at 1.1, 4.2, 77 and 298°K [38].

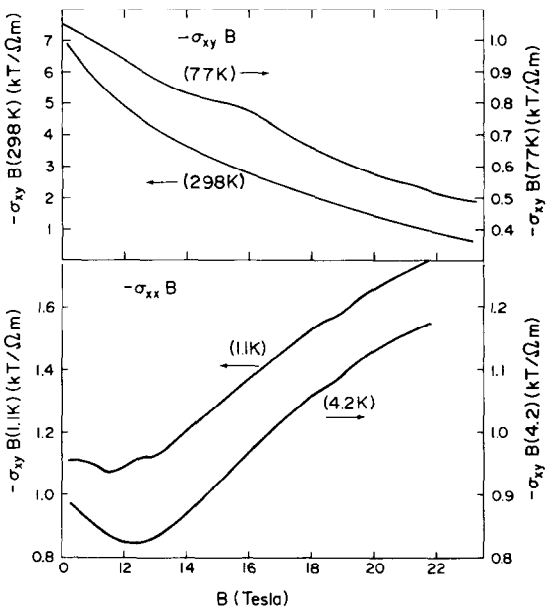

Fig. 19. Curves of $\sigma_{xy}B$ vs B in the quantum limit for HOPG at 1.1, 4.2, 77 and 298°K [38].

A grant from the United States Atomic Energy Commision (1970–76) is gratefully acknowledged. Helpful discussions were also held with Dr. C. Ayache.

REFERENCES

1. I. L. Spain and R. O. Dillon, *Carbon* **14**, 23 (1976).
2. R. O. Dillon, I. L. Spain, J. A. Woollam and W. H. Lowrey, *J. Phys. Chem. Solids* **39**, 923 (1978).
3. R. O. Dillon and I. L. Spain, *J. Phys. Chem. Solids* **19**, 907 (1978).
4. R. O. Dillon, I. L. Spain and J. W. McClure, *J. Phys. Chem. Solids* **39**, 1071 (1978).
5. W. H. Lowrey and I. L. Spain, *Solid-St. Comm.* **22**, 615 (1977). (An extended paper on this work is in preparation).
6. R. O. Dillon and I. L. Spain, *Solid-St. Comm.* **26**, 333 (1978).
7. J. C. Slonczewski and P. R. Weiss, *Phys. Rev.* **109**, 272 (1958).
8. J. W. McClure, *Phys. Rev.* **119**, 606 (1960).
9. J. Inoue, *J. Phys. Soc. Japan* **17**, 808 (1962).
10. R. O. Dillon, I. L. Spain and J. W. McClure, *J. Phys. Chem. Solids* **38**, 635 (1977).
11. I. L. Spain, *Proc. Int. Conf. Semi Metals and Narrow-Band-Gap Semiconductors* (Edited by Carter and Bate), p. 177. Pergamon Press, New York (1971).
12. D. E. Soule, *Phys. Rev.* **112**, 698 (1958).
13. K. Kawamura, N. Sato, T. Tsuzuku, *J. Phys. Soc. Japan* **42**, 5747 (1977).
14. I. L. Spain, A. R. Ubbelohde and D. A. Young, *Phil. Trans. Roy. Soc. (London)* **A262**, 1128 (1967).
15. A review may be found in, A. H. Wilson, *The Theory of Metals*, 2nd Edn. Cambridge University Press (1963).
16. J. W. McClure, *Phys. Rev.* **112**, 715 (1958).
17. J. W. McClure and W. J. Spry, *Phys. Rev.* **165**, 809 (1963).
18. See, J. M. Ziman, *Electrons and Phonons*. Oxford University Press (1960).
19. K. Noto and T. Tsuzuku, *Carbon* **12**, 209 (1974).
20. J. D. Cooper, J. Woore and D. A. Young, *Nature* **225**, 721 (1970).
21. K. Kawamura, N. Sato, T. Aoki and T. Tsuzuku, *J. Phys. Soc. (Japan)* **41**, 2027 (1976).
22. J. A. Woollam, D. J. Sellmyer, R. O. Dillon and I. L. Spain, *Low Temperature Physics-LT*13, (Edited by Timmerhaus, O'Sullivan and Hammel) Vol. 4. p. 358. Plenum Press, New York (1974).
23. L. C. F. Blackman, G. A. Saunders and A. R. Ubbelohde, *Proc. Roy. Soc.* **A264**, 19 (1961).
24. C. A. Klein, *Revs. Mod. Phys.* **34**, 56 (1962).
25. C. A. Klein, *J. Appl. Phys.* **33**, 3338 (1962); **35**, 2947 (1964).
26. C. A. Klein, W. D. Straub and R. J. Diefendorf, *Phys. Rev.* **125**, 468 (1962).
27. A. W. Moore, A. R. Ubbelohde and D. A. Young, *Proc. Roy. Soc. (London)* **A280**, 153 (1964).
28. R. A. Morant, *J. Phys. (London)* **D3**, 1367 (1970).
29. I. L. Spain, *Carbon* **14**, 229 (1976).
30. W. N. Reynolds, *Physical Properties of Graphite*. Elsevier, Amsterdam (1968).
31. L. C. F. Blackman, G. A. Saunders and A. R. Ubbelohde, *Proc. Phys. Soc. (London)* **78**, 1048 (1961).
32. J. D. Cooper, J. P. Smith, J. Woore, D. A. Young, *J. Phys. (London)* **C4**, 442 (1971).
33. J. W. McClure, Proc. *Int. Conf. on Semimetals and Narrow Band-Gap Semiconductors, Dallas*, 1970, p. 127. Pergamon Press, New York (1971).
34. P. R. Schroeder, M. S. Dresselhaus and A. Javan, *Phys. Rev. Letters* **20**, 1292 (1968).
35. I. L. Spain, In *Chemistry and Physics of Carbon* (Edited by P. L. Walker, Jr. and P. A. Thrower), Vol. 8, Chap. 1. Marcel Dekker, New York (1973).
36. D. E. Soule, *IBM, J. Res. Dev.* **8**, 268 (1964).
37. J. A. Woollam, *Phys. Rev.* **B3**, 1148 (1971).
38. W. H. Lowrey and I. L. Spain, *Abstracts of the* 13*th, Biennial Conf. on Carbon, Irvine, Calif.* (1977), p. 58.
39. L. W. Kreps and J. A. Woollam, *Carbon* **15**, 403 (1977).
40. C. Ayache and A. de Combarieu, *Abstracts of the* 13*th Biennial Conference on Carbon, Irvine, Calif.* (1977), p. 60.